Quantum correlations in a noisy neutron interferometer

Christopher J. Wood,[1,2,*] Mohamed O. Abutaleb,[3] Michael G. Huber,[4] Muhammad Arif,[4]
David G. Cory,[1,5,6] and Dmitry A. Pushin[1,2]

[1]*Institute for Quantum Computing, University of Waterloo, Waterloo, Ontario N2L 3G1, Canada*
[2]*Department of Physics and Astronomy, University of Waterloo, Waterloo, Ontario N2L 3G1, Canada*
[3]*Massachusetts Institute of Technology, Cambridge, Massachusetts 02139, USA*
[4]*National Institute of Standards and Technology, Gaithersburg, Maryland 20899, USA*
[5]*Department of Chemistry, University of Waterloo, Waterloo, Ontario N2L 3G1, Canada*
[6]*Perimeter Institute for Theoretical Physics, Waterloo, Ontario N2L 2Y5, Canada*

(Received 30 May 2014; published 15 September 2014)

We investigate quantum coherences in the presence of noise by entangling the spin and path degrees of freedom of the output neutron beam from a noisy three-blade perfect crystal neutron interferometer. We find that in the presence of dephasing noise on the path degree of freedom the entanglement of the output state reduces to 0, however the quantum discord remains nonzero for all noise values. Hence even in the presence of strong phase noise nonclassical correlations persist between the spin and the path of the neutron beam. This indicates that measurements performed on the spin of the neutron beam will induce a disturbance on the path state. We calculate the effect of the spin measurement by observing the changes in the observed contrast of the interferometer for an output beam postselected on a given spin state. In doing so we demonstrate that these measurements allow us to implement a quantum eraser and a which-way measurement of the path taken by the neutron through the interferometer. While strong phase noise removes the quantum eraser, the spin-filtered which-way measurement is robust to phase noise. We experimentally demonstrate this disturbance by comparing the contrasts of the output beam with and without spin measurements of three neutron interferometers with varying noise strengths. This demonstrates that even in the presence of noise that suppresses path coherence and spin-path entanglement, a neutron interferometer still exhibits uniquely quantum behavior.

DOI: 10.1103/PhysRevA.90.032315 PACS number(s): 03.67.Mn, 03.65.Ta, 03.65.Yz, 03.75.Dg

I. INTRODUCTION

A unique property of quantum theory is that when two or more quantum systems are allowed to interact, they may exhibit correlations that cannot be explained classically. In the field of quantum information science, protocols harnessing these correlations can exceed classical efficiencies for certain metrology applications and information processing tasks [1]. One of the most studied classes of correlated quantum states is entangled states, as they enable extremely nonclassical quantum effects such as quantum teleportation [2]. A maximally entangled quantum state of a bipartite quantum system allows for a projective measurement of one subsystem to completely determine the outcome of the corresponding projective measurements on the other. The class of states of interest to quantum computation, however, is broader than purely entangled quantum states, as certain nonentangled quantum states may still possess correlations that cannot be accounted for classically. In such cases measurement on one subsystem, while not determining the state of another, may still cause a disturbance to the state of the other.

Classifying the quantum nature of correlations beyond entanglement has received much interest, with many discussions focused on quantum discord (QD) and related measures [3–5]. QD was proposed by Ollivier and Zurek [6] and Henderson and Vedral [7] to characterize quantum correlations in a bipartite system. In effect, one may interpret QD as a measure of the minimum disturbance that measurement of one subsystem of a bipartite quantum system can induce on the measurement outcomes of the other. Such classifications are of interest since certain quantum algorithms, such as DQC1, do not require entanglement to exceed classical efficiencies [8]. It has been shown that for the DQC1 algorithm QD is present in the output state of the computation even when entanglement is not, and hence it was suggested that QD may provide a better figure of merit for evaluating quantum resources [9]. Here we investigate the quantum nature of correlations of single neutrons in a neutron interferometer (NI).

Neutron interferometry has been used for precise tests of quantum mechanical phenomena such as coherent spinor rotation [10] and superposition [11], gravitationally induced quantum interference [12], the Aharonov-Casher effect [13], violation of a Bell-like inequality [14], generation of a single-neutron entangled state [15], quantum contextuality [16], and the realization of a Decoherence-Free subspace [17]. In our case an NI provides a clean system for considering quantum correlations in a bipartite quantum system, as we are able to coherently control the spin and path-momentum degrees of freedom of a neutron beam and manipulate the correlations between them. In addition, due to the high efficiency of single-neutron detectors and the low intensity of neutrons entering the interferometer, we are able to gather statistics by performing true projective measurements on single quantum systems. In the present article we investigate the correlations between the spin and the path degrees of freedom of the output beam from a noisy NI by observing changes in the output beam intensity as the result of a postselected projective measurement on the neutron spin.

*christopher.j.wood@uwaterloo.ca

II. QUANTUM CORRELATIONS

A. Quantum discord

QD is a nonsymmetrical quantity defined by the difference between quantum generalizations of two classically equivalent expressions for *mutual information*. Let ρ_{AB} be a bipartite density matrix over two quantum systems, A and B. One expression for the mutual information of ρ_{AB} is given by

$$I(A:B) = S(\rho_A) + S(\rho_B) - S(\rho_{AB}), \tag{1}$$

where $S(\rho) = -\mathrm{tr}(\rho \log_2 \rho)$ is the von Neumann entropy of the density matrix ρ, $\rho_A = \mathrm{tr}_B(\rho_{AB})$ is the reduced density matrix on subsystem A taken by performing the partial trace over system B, and similarly, $\rho_B = \mathrm{tr}_A(\rho_{AB})$. An alternative expression for mutual information is formed by considering a quantum generalization of conditional entropy which accounts for possible measurement-induced disturbances. Consider performing a measurement on subsystem B; this is most generally described by a positive operator-valued measure (POVM) E consisting of a set of measurement operators $\{E_b\}$ satisfying $E_b \geqslant 0$, $\sum_b E_b = \mathbf{1}$ [1]. Measurement outcome b will occur with probability $p_b = \mathrm{tr}(E_b \rho_{AB})$, and the postmeasurement state of subsystem A, conditioned on outcome b, is given by

$$\rho_{A|b} = \frac{1}{p_b} \mathrm{tr}_B(E_b \rho_{AB}). \tag{2}$$

We may define a generalization of conditional entropy for a given POVM E as

$$S(\rho_{A|E}) = \sum_b p_b S(\rho_{A|b}). \tag{3}$$

This gives us an alternative expression for mutual information by maximizing over all possible POVMs:

$$J(A|B) = \max_E [S(\rho_A) - S(\rho_{A|E})]. \tag{4}$$

QD is defined to be the difference between expression (1) and expression (4):

$$\begin{aligned} D(A|B) &= I(A:B) - J(A|B) \\ &= \min_E [S(\rho_{A|E}) + S(\rho_B) - S(\rho_{AB})]. \end{aligned} \tag{5}$$

Similarly one may define the QD $D(B|A)$ where one optimizes over POVMs on subsystem B. In general, to compute the QD of a state one must minimize Eq. (5) over all extremal rank 1 POVMs, however, it has been shown that for rank 2 states orthogonal projective valued measurements are optimal [18].

B. Entanglement of formation

There are numerous measures for quantifying entanglement in a quantum state (for a review of entanglement see [2]). In our case a convenient measure for a two-qubit mixed state is the *entanglement of formation* (EOF) [19], which is given by

$$\mathrm{EOF}(\rho_{AB}) = h\left(\frac{1 + \sqrt{1 - \mathcal{C}(\rho_{AB})^2}}{2}\right), \tag{6}$$

where $h(x) = -x \log_2 x - (1-x)\log_2(1-x)$, and $\mathcal{C}(\rho_{AB})$ is the *concurrence* of a bipartite state ρ_{AB},

$$\mathcal{C}(\rho_{AB}) = \max\{0, \lambda_1 - \lambda_2 - \lambda_3 - \lambda_4\}, \tag{7}$$

where λ_j are the eigenvalues of the Hermitian matrix

$$\sqrt{\sqrt{\rho_{AB}}(Y \otimes Y)\rho_{AB}^*(Y \otimes Y)\sqrt{\rho_{AB}}} \tag{8}$$

sorted such that $\lambda_1 \geqslant \lambda_2 \geqslant \lambda_3 \geqslant \lambda_4$, where the asterisk denotes complex conjugation, and Y is the Pauli Y matrix.

C. Quantum correlations in a neutron interferometer

We now consider quantum correlations in the output state of a three-blade NI and will follow with the mathematical model of the NI used to derive them in Sec. III. In our configuration systems, A and B correspond to the path and spin degrees of freedom of a neutron, respectively, which each may be modeled as a two-level quantum system (qubit). By performing a controlled spin rotation of angle $0 \leqslant \alpha \leqslant 2\pi$ in one of the paths of the NI we may introduce entanglement between the spin and the path subsystems of an initially spin-polarized neutron beam. In a realistic NI there are noise sources which introduce decoherence and reduce the effectiveness of this entangling operation. In the present paper we consider decoherence due to surface defects of the NI blades. This noise source introduces a random phase between the two interferometer paths which degrades the coherence of the path subsystem A.

Since the neutrons exiting the NI may be described by a mixed state of a two-qubit quantum system, we use the EOF as a measure of the entanglement in the output state. Further, since the quantum state of the neutrons is rank 2 we need only perform the minimization in Eq. (5) over projective valued measurements on the spin subsystem to calculate the QD. We find that the EOF between the spin and the path systems goes to 0 asymptotically as the strength of the random phase noise increases, while the QD remains nonzero for all values of the spin rotation except $n\pi$ for integer values of n. This is illustrated in Fig. 1. Even though there is no entanglement between the spin and the path of the neutrons in the case of strong phase noise, the nonzero QD $D(A|B)$ indicates the presence of nonclassical correlations. This signifies that measurements performed on the neutron spin will induce a disturbance in the path state of the output neutron beam.

The observed entanglement evolution under an increase in the strength of the phase noise can be classed as *approaching* [20], in contrast to entanglement sudden death [21]. QD has been shown to be robust to sudden death and instead asymptotically vanishes in bipartite systems subject to Markovian evolution [22,23], however, in our case QD remains asymptotically nonzero for most spin rotation values. Similar effects of the vanishing of entanglement but nonvanishing QD have been previously found in the theoretical analysis of the evolution of coupled quantum dots under decoherence [24]. Certain initially correlated two-atom states have also been shown to have a nonvanishing QD when coupled to a common dissipative cavity [25].

III. THEORETICAL MODEL

We now briefly describe the mathematical model used to describe the NI. The most common geometry for a NI is a three-blade system machined from a perfect single crystal of silicon. This functions as a Mach-Zehnder interferometer on

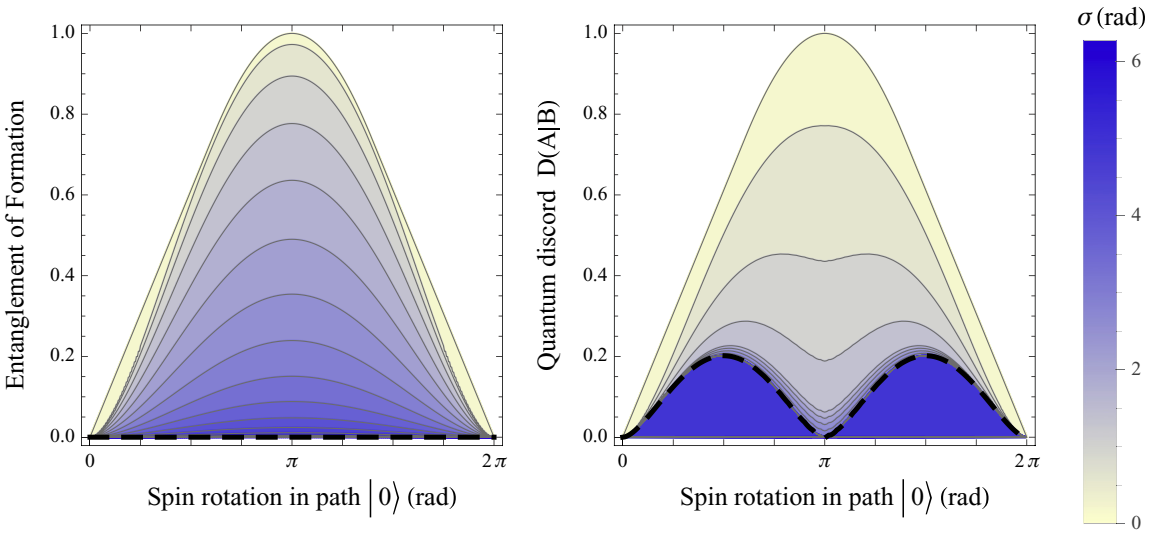

FIG. 1. (Color online) Entanglement of formation (left) and quantum discord $D(A|B)$ (right) between the spin and the path degrees of freedom of neutrons exiting a three-blade NI, as a function of the spin rotation angle of neutrons in the $|0\rangle$ interferometer path, and the noise strength σ. The NI schematic is shown in Fig. 2, and the noise model considered introduces a normally distributed random phase, with mean 0 and standard deviation σ, between the NI paths. The dashed line corresponds to the maximum noise case of a uniform distribution of angles. While the entanglement approaches 0 for all spin rotation angles as the noise strength increases, the quantum discord remains nonzero.

the longitudinal momentum of the neutron beam. We refer to this degree of freedom of the neutron beam as the *path* system. The neutron path can be viewed as a two-level system which we may couple to the neutron spin to form a bipartite quantum system. In this context we may view the interferometer crystal as a quantum circuit acting as illustrated in Fig. 2. We define the basis for the path to be the computational basis where $|0\rangle$ and $|1\rangle$ correspond to the red and blue beam paths in Fig. 2, respectively. For the spin system we work in the spin-up, spin-down eigenbasis $|\uparrow\rangle, |\downarrow\rangle$ with respect to a static field in the z direction.

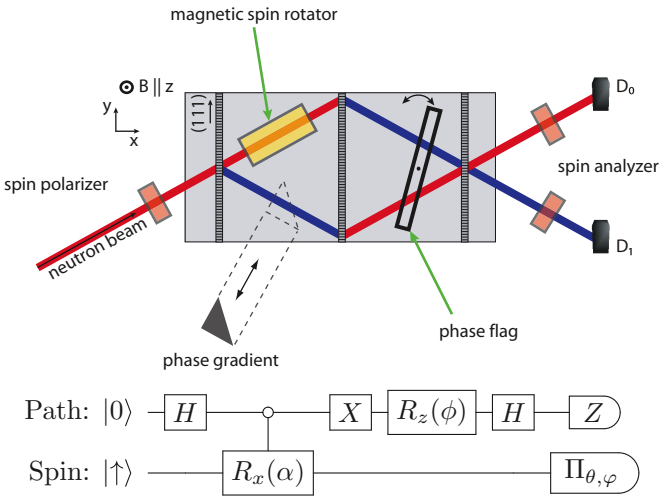

FIG. 2. (Color online) Experimental setup for the three-blade neutron interferometer (top) and the corresponding quantum circuit for the ideal model (bottom). The red (blue) paths in the NI schematic are defined as the $|0\rangle(|1\rangle)$ path states, H is a Hadamard gate, $R_x(\alpha)$ is a rotation of the neutron spin in the $|0\rangle$ path of α radians about the x axis, X is a bit flip, $R_z(\phi)$ is a relative phase shift of ϕ radians between the beam paths, Π is a projective measurement performed on the spin state (spin analyzer) in the basis $\cos(\theta)|\uparrow\rangle \pm e^{i\varphi}\sin(\theta)|\downarrow\rangle$, and Z is a projective measurement of the path intensities in the $|0\rangle, |1\rangle$ basis.

The first (and third) NI blades act as Hadamard (H) gates on the neutron path by coherently splitting (and recombining) the neutron beam into two paths via Bragg scattering in the Laue geometry [26]. The second NI blade deflects the beam by swapping the path-momentum directions, which we model as a bit-flip (X) gate. In our defined bases these are given by

$$H = \frac{1}{\sqrt{2}}\left(|0\rangle\langle 0| + |0\rangle\langle 1| + |1\rangle\langle 0| - |1\rangle\langle 1|\right), \tag{9}$$

$$X = |0\rangle\langle 1| + |1\rangle\langle 0|. \tag{10}$$

In practice, the intensity of the output neutron beam is reduced due to neutrons escaping the NI at the second blade, however, we account for this in our description of the output beam by postselecting on the neutrons which remain in the interferometer.

Between the first and the second NI blades we couple the spin and path degrees of freedom by selectively rotating the neutron spin in the $|0\rangle$ path by an angle α. This acts as a controlled-X rotation $[R_x(\alpha)]$, with the spin and path as the target and control, respectively:

$$\text{C-}R_x(\alpha) = |0\rangle\langle 0| \otimes R_x(\alpha) + |1\rangle\langle 1| \otimes \mathbf{1}_s, \tag{11}$$

$$R_x(\alpha) = \exp\left[i\,\frac{\alpha}{2}\left(|\uparrow\rangle\langle\downarrow| + |\uparrow\rangle\langle\downarrow|\right)\right], \tag{12}$$

$$\mathbf{1}_s = |\uparrow\rangle\langle\uparrow| + |\downarrow\rangle\langle\downarrow|. \tag{13}$$

We measure the intensities of the output beams using two ^{3}He integrating detectors called D_0 and D_1, corresponding to projective measurements of states $|0\rangle$ and $|1\rangle$, respectively. This performs a Z-basis measurement on the neutron path

subsystem. By including spin filters which selectively transmit neutrons with a preferred spin we may also perform postselected spin measurements. This allows us to perform joint measurements on the spin and path of the neutron beam.

In a typical NI experiment a relative phase of ϕ is induced between the two paths by a phase flag between the second and the third blades which effectively implements the Z-rotation gate:

$$R_z(\phi) = e^{-i\phi/2}|0\rangle\langle 0| + e^{i\phi/2}|1\rangle\langle 1|. \tag{14}$$

The relative phase ϕ parameterizes the measured beam intensity by controlling the interference between the two beam paths recombined at the third blade.

Ideally the input beam is in the spin-up polarized state $\psi_{\text{in}} = |0\rangle \otimes |\uparrow\rangle$ with respect to a uniform magnetic field in the z direction. In practice, however, one is not able to perfectly polarize the input neutron beam and in general we describe the input beam by the state

$$\rho_{\text{in}}(\epsilon) = |0\rangle\langle 0| \otimes \left(\frac{1+\epsilon}{2}|\uparrow\rangle\langle\uparrow| + \frac{1-\epsilon}{2}|\downarrow\rangle\langle\downarrow|\right), \tag{15}$$

where $-1 \leqslant \epsilon \leqslant 1$ parameterizes the spin polarization of the neutron beam.

A. Output intensities

In an ideal NI interference effects are observed in the measured output intensity at each detector. The ideal output intensity is a function of the relative phase between interferometer paths and the angle of spin rotation in the $|0\rangle$ path. If no measurement is performed on the neutron spin subsystem, the ideal detector probabilities in the absence of noise are given by

$$\begin{aligned} D_{0,\text{Ideal}}(\phi,\alpha) &= \frac{1}{2}\left[1 + \cos\left(\frac{\alpha}{2}\right)\cos(\phi)\right], \\ D_{1,\text{Ideal}}(\phi,\alpha) &= \frac{1}{2}\left[1 - \cos\left(\frac{\alpha}{2}\right)\cos(\phi)\right], \end{aligned} \tag{16}$$

which are independent of the spin-polarization of the neutron beam. In a real NI the blades do not generally have equal transmission and reflection coefficients and hence are not true 50-50 beam splitters. This does not affect the interference effects at detector D_0, however, since both interferometer paths to this detector have the same number of transmissions and reflections.

In practice, NIs cannot be machined perfectly and surface imperfections in the crystal blades lead to a distribution of phases over the cross-sectional area of the neutron beam. This results in reduced contrast of the beam intensity when averaged over the beam distribution. To include the effect of phase noise in our model we consider the output intensities with a phase shift $\phi + \phi_r$, where ϕ_r is an additional random phase shift introduced between paths by the NI blades. This random phase is assumed to be normally distributed, with mean 0 and variance σ. By averaging over the distribution of ϕ_r, we may obtain the average detector intensities:

$$\begin{aligned} D_0(\phi,\alpha,\sigma) &= \int_{-\infty}^{\infty} d\phi_r\, D_{0,\text{Ideal}}(\phi+\phi_r,\alpha)\,\frac{\exp\left(-\frac{\phi_r^2}{2\sigma^2}\right)}{\sqrt{2\pi\sigma^2}}, \\ D_0(\phi,\alpha,\sigma) &= \frac{1}{2}\left[1 + e^{-\sigma^2/2}\cos\left(\frac{\alpha}{2}\right)\cos(\phi)\right]. \end{aligned} \tag{17}$$

1. Output intensity with spin filtering

We now consider the detector intensities when we include a spin filter to perform a postselected spin measurement on the output neutron beam before detector D_0. The spin filter implements a postselected projective measurement of the pure state

$$|S(\theta,\varphi)\rangle = \cos\left(\frac{\theta}{2}\right)|\uparrow\rangle + e^{i\varphi}\sin\left(\frac{\theta}{2}\right)|\downarrow\rangle, \tag{18}$$

where θ and φ are the spherical coordinates parameterizing the state on the Bloch sphere. In practice, the spin filter acts by absorbing neutrons in the orthogonal spin state before they reach the detector. After postselection the detector intensity is proportional to

$$\begin{aligned} &D_{0,S(\theta,\varphi)}(\phi,\alpha,\sigma,\epsilon) \\ &= \frac{1}{4}\Big(1 + \epsilon\cos^2(\alpha/2)\cos(\theta) + \frac{\epsilon}{2}\sin(\alpha)\sin(\theta)\sin(\varphi) \\ &\quad + e^{-\frac{\sigma^2}{2}}\cos(\alpha/2)(1+\epsilon\cos(\theta))\cos(\phi) \\ &\quad - e^{-\frac{\sigma^2}{2}}\sin(\alpha/2)\sin(\theta)\cos(\phi)[\sin(\phi) - \epsilon\sin(\varphi)]\Big). \end{aligned} \tag{19}$$

We explicitly consider two cases: spin filtering in the same axes as the quantizing magnetic field (Z filter) and spin-filtering in an orthogonal basis (X filter). These are given by

$$\begin{aligned} Z &: |\uparrow\rangle = |S(0,0)\rangle, \quad |\downarrow\rangle = |S(\pi,0)\rangle, \\ X &: |\uparrow_x\rangle = |S(\pi/2,0)\rangle, \quad |\downarrow_x\rangle = |S(3\pi/2,0)\rangle \end{aligned} \tag{20}$$

in terms of the (θ,ϕ) parametrization in (18).

In these cases of the Z filter the observed intensities at detector D_0 are proportional to

$$D_{0,\uparrow z}(\phi,\alpha,\sigma,\epsilon) = \left(\frac{1+\epsilon}{2}\right) D_0(\phi,\alpha,\sigma) + \frac{\epsilon}{8}\left[\cos(\alpha) - 1\right], \tag{21}$$

$$D_{0,\downarrow z}(\phi,\alpha,\sigma,\epsilon) = \left(\frac{1-\epsilon}{2}\right) D_0(\phi,\alpha,\sigma) - \frac{\epsilon}{8}\left[\cos(\alpha) - 1\right] \tag{22}$$

for spin-up and spin-down filtering in the z direction, respectively. Note that in this case the normalization condition for the output probabilities is that $D_{0,\downarrow} + D_{0,\uparrow} + D_{1,\downarrow} + D_{1,\uparrow} = 1$.

In these cases of the X filter the observed intensities at detector D_0 are proportional to

$$D_{0,\uparrow x}(\phi,\alpha,\sigma) = \frac{1}{4}\left[1 + e^{-\sigma^2/2}\cos\left(\frac{\alpha}{2}+\phi\right)\right], \quad (23)$$

$$D_{0,\downarrow x}(\phi,\alpha,\sigma) = \frac{1}{4}\left[1 + e^{-\sigma^2/2}\cos\left(\frac{\alpha}{2}-\phi\right)\right] \quad (24)$$

for spin-up and spin-down filtering in the x direction, respectively. We see here that the Z filter adds an additional term to the unfiltered contrast, while the X filtering combines the parameters ϕ and α into a single argument of a cosine function. Further, in the weak-noise case ($\sigma \approx 0$) both these expressions are observably different from the non-spin-filtered case in Eq. (17). However in the case of strong noise, the non-spin-filtered and X-filtered intensities approach constant values. Only the Z-filtered intensities are observably different from the non-spin-filtered intensity and depend on the initial spin polarization ϵ and the controlled spin-rotation angle α. We discuss the implications of these results in Sec. IV, but first we introduce a measure of coherence in interferometer experiments called *contrast*.

B. Contrast

The intensity curves for each detector as a function of the relative phase ϕ between interferometer paths are referred to as *contrast curves*. They are analogous to the interference pattern produced by a double-slit interference experiment. The difference between the maximum and the minimum intensity of the D_0 detector as a function of a phase-flag rotation ϕ is called the contrast of the NI and is defined as

$$C_P = \frac{\max_\phi[D_0(\phi)] - \min_\phi[D_0(\phi)]}{\max_\phi[D_0(\phi)] + \min_\phi[D_0(\phi)]}. \quad (25)$$

The contrast may take values $0 \leqslant C_P \leqslant 1$ and is a measure of the strength of quantum coherence between the paths.

We also consider an alternative contrast expression where our parameter of variation in detector intensity is the angle of spin rotation α rather than the phase rotation ϕ as in Eq. (25). We define the *spin contrast* to be given by

$$C_S = \frac{\max_\alpha[D_0(\alpha)] - \min_\alpha[D_0(\alpha)]}{\max_\alpha[D_0(\alpha)] + \min_\alpha[D_0(\alpha)]}. \quad (26)$$

We refer to the standard contrast as the *path contrast*, to distinguish it from the spin contrast.

1. Contrast without spin filtering

Using the observed detector probability in Eq. (17) we may calculate the path and spin contrasts of the noisy three-blade NI:

$$C_P(\alpha,\sigma) = e^{-\sigma^2/2}\left|\cos\left(\frac{\alpha}{2}\right)\right|, \quad (27)$$

$$C_S(\phi,\sigma) = e^{-\sigma^2/2}\,|\cos(\phi)|. \quad (28)$$

We see here that the average path contrast and spin-contrast expressions are equivalent, but with the roles of α and ϕ interchanged ($C_S(\phi,\sigma) = C_P(2\phi,\sigma)$), and depend on the noise strength and the phase of the parameter that is not optimized over for the contrast (α for path contrast and ϕ for spin contrast).

2. Contrast with spin filtering

We now consider the theoretical path and spin contrasts of the output beam after spin filtering. When we postselect on the spin-up and spin-down states of the X filter we obtain contrast values of

$$C_{P(\uparrow x)}(\sigma) = C_{S(\uparrow x)}(\sigma) = e^{-\sigma^2/2}, \quad (29)$$

$$C_{P(\downarrow x)}(\sigma) = C_{S(\downarrow x)}(\sigma) = e^{-\sigma^2/2}. \quad (30)$$

We find that the spin and path contrasts are equivalent and depend only on the strength of the phase noise. In particular, the contrast decreases to 0 with an increase in noise strength.

For the Z-filtered intensities we obtain postselected path contrasts of

$$C_{P(\uparrow z)}(\alpha,\sigma,\epsilon) = \left|\frac{(1+\epsilon)e^{-\sigma^2/2}\cos\left(\frac{\alpha}{2}\right)}{1+\frac{\epsilon}{2}(1+\cos(\alpha))}\right|, \quad (31)$$

$$C_{P(\downarrow z)}(\alpha,\sigma,\epsilon) = \left|\frac{(1-\epsilon)e^{-\sigma^2/2}\cos\left(\frac{\alpha}{2}\right)}{1-\frac{\epsilon}{2}(1+\cos(\alpha))}\right|, \quad (32)$$

which satisfy

$$C_{P(\uparrow z)}(\alpha,\sigma,\epsilon) \geqslant C_P(\alpha,\sigma) \geqslant C_{P,\downarrow z}(\alpha,\sigma,\epsilon) \quad (33)$$

for $\epsilon \geqslant 0$, with equality in the case of a zero spin polarization ($\epsilon = 0$). In particular, we see that $C_{\text{path},\downarrow z}(\alpha,\sigma,1) = 0$.

The spin contrasts for the Z-filtered intensities are more complicated, as the values of α which obtain the minimum for the detector intensities are, in general, functions of ϕ, ϵ, and σ. For the spin-up Z filter we have

$$C_{S(\uparrow z)}(\phi,\sigma,\epsilon) = \frac{\epsilon + (1+\epsilon)C_S(\phi,\sigma) + C_S(\phi,\sigma)^2}{2+\epsilon+(1+\epsilon)C_S(\phi,\sigma) - C_S(\phi,\sigma)^2}. \quad (34)$$

For the spin-down Z filter, in the range of $\frac{1}{3} \leqslant \epsilon \leqslant 1$, we have

$$C_{S(\downarrow z)}(\phi,\sigma,\epsilon) = \frac{\epsilon - (1-\epsilon)C_S(\phi,\sigma) + \frac{(1-\epsilon)^2}{4\epsilon}C_S(\phi,\sigma)^2}{2-\epsilon+(1-\epsilon)C_S(\phi,\sigma) - \frac{(1-\epsilon)^2}{4\epsilon}C_S(\phi,\sigma)^2}. \quad (35)$$

For the specific case of unpolarized neutrons ($\epsilon = 0$) we have

$$C_{S(\uparrow z)}(\phi,\sigma,0) = C_{S(\downarrow z)}(\phi,\sigma,0) = C_S(\phi,\sigma), \quad (36)$$

and in the case of perfect polarization ($\epsilon = 1$) we find that for spin-down Z filtering we have perfect spin contrast:

$$C_{S(\downarrow z)}(\phi,\sigma,1) = 1. \quad (37)$$

In the case of strong noise the Z-filtered spin-contrast expressions reduce to

$$C_{S(\uparrow z)}(\phi,\infty,\epsilon) = \frac{\epsilon}{2+\epsilon}, \quad (38)$$

$$C_{S(\downarrow z)}(\phi,\infty,\epsilon) = \frac{\epsilon}{2-\epsilon} \quad (39)$$

and depend only on the initial polarization ϵ of the neutron beam. In practice, strong noise amounts to $\sigma \geqslant 2\pi$.

IV. INTERPRETATION AND PROPOSED EXPERIMENTS

We now discuss the significance of previously calculated path-constrast and spin-contrast values for the noisy three-blade NI. In the absence of spin filtering, while both the path contrast and the spin contrast of the ideal three-blade NI go to 0 as the noise strength σ increases, as shown in Fig. 1, there is a nonzero QD $D(A|B)$ between the spin and the path subsystems. This implies that if we implement a measurement on the spin system, the output intensities of the path system must be affected. By using a spin filter we are able to postselect on an outcome arbitrary projective valued measurement on the spin neutron system, however, to observe the influence of the spin filter we are restricted by being able to measure the path subsystem only in the $|0\rangle,|1\rangle$ basis due to the inability to change the final blade of the NI. Hence when we are restricted to a single-measurement basis this influence may not be observable for all spin postselected states.

A. No spin postselection

In the absence of spin filtering we found the path contrast for the noisy NI as given in Eq. (27), dependent only on the noise strength σ and the angle of controlled spin rotation α. In the absence of noise, as we increase the angle of spin rotation up to $\alpha = \pi$ the measured contrast reduces to 0. At $\alpha = \pi$ the spin and path subsystems are maximally entangled, as shown by the EOF of 1 in Fig. 1. By not measuring the spin subsystem we can partially trace over this subsystem, which, in the case of a maximally entangled state, results in a maximally mixed reduced state of the path subsystem and, hence, zero contrast. This may be interpreted as having performed a *which-way* measurement of the path taken by the neutron through the interferometer. The neutrons passing the spin filter are marked to have spin-down, while the neutrons which do not go through the arm with the spin rotator will all have spin-up. By tuning $0 < \alpha < \pi$ we can control the strength of this which-way marking of the neutrons. For α close to 0 it becomes a weak which-way marking of the path taken by the neutrons through the interferometer, and hence we still retain some contrast.

In the case of spin contrast, as given in Eq. (28), we have the same situation, but with the roles of the rotation angle α and phase flag ϕ reversed. In this case we are doing a spin-based magnetic interference experiment, and the relative phase between paths now performs the which-way marking of the neutron. In both cases the presence of noise reduces the value of contrast, until it is approximately 0 at $\sigma = 2\pi$. This would suggest that the random-phase noise destroys all relative phase information, and hence coherence, between the two paths in the interferometer. However, due to the nonzero discord between the path and the spin of the neutron we may attempt to recover some information by spin measurements.

1. X filter spin postselection

In the case of X filtering we found that both the path contrast and the spin contrast when spin filtering on the $|\uparrow_x\rangle$ or $|\downarrow_x\rangle$ spin states depended only on the strength σ of the random-phase noise, as shown in Eq. (29). This is because the X-filter postselection acts to combine the parameters α and ϕ into a single relative phase parameter $\phi + \alpha/2$ between the two NI paths which is observed at the detector. For path contrast the spin rotation angle only shows up as a shift in the contrast curves, without changing the actual contrast value. In effect, the X filter has erased the which-way marking of the neutrons in the NI due to the controlled spin-rotation angle. Similarly, for the spin contrast the roles of ϕ and α are swapped with the spin filter now, erasing all effect of the phase-flag parameter on the output intensities. This is analogous to a *quantum eraser* in optics [27]. By postselecting on the neutron spin in the x direction we have erased the which-way measurement caused by entanglement between the spin and the path neutron subsystems. However, as the noise strength increases the spin-filtered spin and path contrasts, both decrease to 0 and become indistinguishable form the unfiltered contrast.

2. Z filter spin postselection

When implementing a Z-filter postselection we calculated quite different values for the spin contrast and path contrast. In the case where we postselect on the $|\uparrow\rangle$ spin state, the path contrast in Eq. (31) is maximized for a perfectly polarized input ($\epsilon = 1$), as we are, in effect, filtering out only the portion of neutrons rotated away from $|\uparrow\rangle$ by the spin rotator. In this sense, much like the nonpostselected case, the angle of rotation controls the strength of the which-way measurement. If instead we filter on $|\downarrow\rangle$ as given by Eq. (32), then we find that the contrast is 0 for $\epsilon = 1$. This is because in this case we are postselecting only on the spins that were rotated, and hence we are performing a perfect which-way measurement of the path taken by the neutrons and cannot have any path-based interference effects. If the incoming beam is not perfectly polarized, our which-way measurement is effectively noisy and we have a fraction of unrotated neutrons that still have spin-down polarization. In this case, as with the $|\uparrow\rangle$ filter, the angle of rotation α controls the relative strength of the which-way measurement.

For the spin-filtered spin contrast we find that with perfect polarization the spin-filtered contrast with spin-down postselection is always 1. However, with $\epsilon < 1$ the value of contrast will depend on the phase flag ϕ, which acts as the which-way marking. As with the unfiltered case it will be maximum for $\phi = 0$ and 0 at $\phi = \pi/2$.

As the noise strength increases, the dependence of ϕ is removed, as we are decohering the relative phase information between paths. Hence the noise is erasing the which-way marking due to the phase flag on the spin contrast. In the strong-noise case we find that the spin contrast depends only on the initial polarization ϵ. If $\epsilon = 1$, we are filtering out all spins that are not rotated to $|\downarrow\rangle$, so our measured intensity is a function of the rotation angle. In the $\epsilon < 1$ case, we are effectively introducing spin noise into the system, as there will now be a $(1-\epsilon)/2$ portion of neutrons with spin-down in the nonrotated path, thus reducing the spin contrast. For the spin-up filter we have a similar situation, however, the contrast is no longer unity for $\epsilon = 1$ unless $\phi = 0$ and $\sigma = 0$. In this case we are filtering out the percentage of neutrons rotated

to spin-down by the spin rotator, rather than postselecting on them.

It has been suggested that this setup might be used to demonstrate the so-called *quantum Cheshire cat* paradox [28]. This paradox is to weakly perform two measurements of the path a neutron takes through the interferometer simultaneously: one that is spin based and determines that the neutron spin goes down one arm of the interferometer and another that is not spin based and determines that the neutron itself went down the other interferometer arm. By doing the which-way marking with a spin filter we may measure which path the neutron spin went down by a spin-based measurement. By varying α we may control the strength of this measurement. To complete the experiment would require implementing a second weak measurement simultaneously to suggest that the neutron itself was observed to go down a different path from its spin degree of freedom. This has been suggested to be implemented in an NI by using a partial absorber in the interferometer path without the spin rotator [29].

V. EXPERIMENTAL DEMONSTRATION

We were able to experimentally demonstrate some of the theoretical results from Sec. III B. However, temperature variations caused by the the method of implementing the spin rotator resulted in a phase drift which increases the effective strength of the phase noise in our NI. Hence while we can calculate path contrast in the absence of spin rotation, for the spin-contrast experiments the spin rotator acts to increase the apparent phase noise so that $e^{-\sigma^2/2} \approx 0$. With the increase in phase noise the spin contrast with no spin filtering, and with X filtering, is expected to be approximately 0. We may only observe the Z-filtered contrast, which, in the strong-noise case, depends only on the neutron polarization. This Z-filter postselection demonstrates the disturbance of the path state of the neutrons by measurement of the neutron spin in the presence of strong noise, as indicated by the nonzero QD as shown in Fig. 1.

A. Experimental setup

We compared the contrast and spin-filtered contrasts after postselecting on spin-down neutrons, quantized in a static magnetic field in the z direction, for three NIs using the setup shown in Fig. 2. The experiment was performed at the National Institute of Standards and Technology Center for Neutron Research's Neutron Optics and Interferometer Facility, located in Gaithersburg, Maryland [30]. This facility has an excellent vibration isolation, and temperature stability thus allows for good and long phase stability [31].

Our neutron beam consisted of 0.271-nm-wavelength neutrons, and the incident neutron beam was polarized via a transmission-mode supermirror polarizer [32], giving an initial polarization of 93% spin-up. The path-selective spin rotation was implemented using thin permalloy films [33] deposited on a Si substrate [34]. Spin filters were implemented using either Heusler crystals or reflection-mode curved supermirrors. These were preceded by an adiabatic coil used to rotate the neutron spin so that spin-up neutrons were absorbed and spin-down neutrons were transmitted. During this experimental

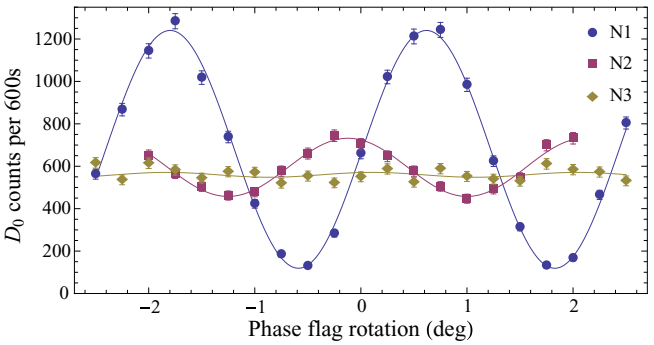

FIG. 3. (Color online) Measured intensity curves at detector D_0 as a function of phase-flag rotation for three NIs. The corresponding path-contrast values are $C_{P1} = (82.5 \pm 1.3)\%$, $C_{P2} = (23 \pm 1.5)\%$, and $C_{P3} = (2 \pm 1.7)\%$ for interferometers N_1, N_2, and N_3, respectively.

work we have used two LLL-type NIs with different initial contrasts, "good" and "bad," which we refer to as N_1 and N_2, respectively. To compare spin contrast with a very low-contrast NI under the same environmental conditions we used the good NI and introduced a large destructive phase gradient by adding a 45° fused silica wedge in one interferometer path [35]. We refer to the good NI with the wedge as N_3.

B. Results

The measured contrast curves in the absence of spin filtering for the three NIs is shown in Fig. 3; these correspond to contrast values of $C_{P1} = (82.5 \pm 1.3)\%$, $C_{P2} = (23 \pm 1.5)\%$, and $C_{P3} = (2 \pm 1.7)\%$ for interferometers N_1, N_2, and N_3, respectively. These contrast values correspond to standard deviations of $\sigma_1 = 0.62 \pm 0.03$, $\sigma_2 = 1.71 \pm 0.04$, and $\sigma_3 = 2.80 \pm 0.61$, respectively, in the noise model under consideration.

After application of the spin-down filter, the spin-filtered contrasts were found to be $C_{S1(\downarrow z)} = (78.0 \pm 3)\%$, $C_{S2(\downarrow z)} = (74.2 \pm 2.2)\%$, and $C_{S3(\downarrow z)} = (84 \pm 4)\%$, as shown in Fig. 4.

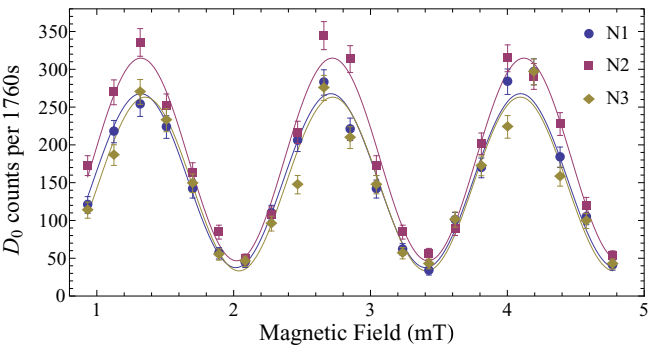

FIG. 4. (Color online) Measured intensity curves at detector D_0 as a function of spin rotation for three NIs, where we have applied a spin filter on the output beam to select spin-down neutrons with respect to a static magnetic field in the z direction. The corresponding spin-contrast values are $C_{S1(\downarrow z)} = (78.0 \pm 3)\%$, $C_{S2(\downarrow z)} = (74.2 \pm 2.2)\%$, and $C_{S3(\downarrow z)} = (84 \pm 4)\%$ for interferometers N_1, N_2, and N_3 respectively.

Our theoretical model, with an initial neutron spin polarization of $(1+\epsilon)/2 = 93\%$, predicts a spin contrast of 75.3% for all three interferometers.

VI. CONCLUSION

We have theoretically and experimentally investigated the role of quantum correlations in a simple bipartite quantum system in the presence of noise by using the spin and path degrees of freedom of a polarized neutron beam in an NI. If we initially entangle the path and spin degrees of freedom of a neutron beam by a path-dependent spin rotation, we find that phase noise acts to reduce the amount of entanglement to 0 as the noise strength increases. However, a nonzero value of QD $D(A|B)$ for all noise strengths indicates that there are still nonclassical correlations between the neutron spin and the neutron path degrees of freedom. The nonzero QD indicates that spin measurements will have an influence on the quantum state of the neutron path subsystem, however, due to the experimental limitations we are only able to perform measurements of the path subsystem in the basis corresponding to the beam paths as implemented by the physical neutron detectors. Restricted to this measurement basis, we are not able to see a noticeable effect for all projective measurements in the strong-noise limit.

In the low-noise case our analysis showed that we may think of the spin-path NI as a quantum eraser. In the absence of spin filtering, by rotating the spin state of a neutron in only one path of the interferometer we are labeling the neutrons which take this path and performing a which-way measurement of the neutron's path though the interferometer. This results in a loss of contrast proportional to the entanglement of the path and neutrons. By implementing a postselected spin measurement in the x direction we may erase this labeling data and restore contrast. This also holds true for the spin contrast, but with the roles of the phase flag and controlled spin rotation angle interchanged. However, in the strong-noise case, the X-filtered path and spin contrast both decrease to 0 and so are not observably different from the non-spin-filtered contrast. Thus the effect of x-basis spin measurements on the path subsystem state are not directly observable in the NI in the presence of strong dephasing noise.

In the case of spincontrast with postselected spin measurement in the z direction, the contrast remains a function of the spin rotation angle but removes the effect of the phase noise. In the high-noise case the expression for spin contrast when we perform a Z filter and postselect on the spin-down state is a function of spin polarization only. Hence even in the high-noise case we are able to experimental observe the effect of spin filtering on the path subsystem. Our experimental results agree with our theoretical model predicting an increase in spin-filtered contrast over phase contrast for three NIs when spin filtering has been performed on the spin-down state in the z direction. The deviations between our measured spin-filtered contrast and the value predicted by our theoretical model are consistent with phase variations over the acquisition time due to temperature and humidity fluctuations in the NI environment. We interpret this nonzero QD as a signature that, even in the presence of strong phase noise, the NI still exhibits genuine quantum behavior.

ACKNOWLEDGMENTS

The authors gratefully acknowledge useful discussions with R. Pynn and G.-X. Miao and the use of permalloy films from M. Th. Rekveldt and R. Pynn. This work was supported by the Canadian Excellence Research Chairs (CERC) program, the Canadian Institute for Advanced Research (CIFAR), the Natural Sciences and Engineering Research Council of Canada (NSERC), the Collaborative Research and Training Experience Program (CREATE), Industry Canada, and the Province of Ontario.

[1] M. A. Nielsen and I. L. Chuang, *Quantum Computation and Quantum Information* (Cambridge University Press, Cambridge, 2000).
[2] R. Horodecki, P. Horodecki, M. Horodecki, and K. Horodecki, Rev. Mod. Phys. **81**, 865 (2009).
[3] M. D. Lang, C. M. Caves, and A. Shaji, Int. J. Quantum Inform. **09**, 1553 (2011).
[4] L. C. Céleri, J. Maziero, and R. M. Serra, Int. J. Quantum Inform. **09**, 1837 (2011).
[5] K. Modi, A. Brodutch, H. Cable, T. Paterek, and V. Vedral, Rev. Mod. Phys. **84**, 1655 (2012).
[6] H. Ollivier and W. H. Zurek, Phys. Rev. Lett. **88**, 017901 (2001).
[7] L. Henderson and V. Vedral, J. Phys. A **34**, 6899 (2001).
[8] E. Knill and R. Laflamme, Phys. Rev. Lett. **81**, 5672 (1998).
[9] A. Datta, A. Shaji, and C. M. Caves, Phys. Rev. Lett. **100**, 050502 (2008).
[10] H. Rauch, A. Zeilinger, G. Badurek, A. Wilfing, W. Bauspiess, and U. Bonse, Phys. Lett. A **54**, 425 (1975).
[11] J. Summhammer, G. Badurek, H. Rauch, U. Kischko, and A. Zeilinger, Phys. Rev. A **27**, 2523 (1983).
[12] R. Colella, A. W. Overhauser, and S. A. Werner, Phys. Rev. Lett. **34**, 1472 (1975).
[13] A. Cimmino, G. I. Opat, A. G. Klein, H. Kaiser, S. A. Werner, M. Arif, and R. Clothier, Phys. Rev. Lett. **63**, 380 (1989).
[14] Y. Hasegawa, R. Loidl, G. Badurek, M. Baron, and H. Rauch, Nature **425**, 45 (2003).
[15] Y. Hasegawa, R. Loidl, G. Badurek, S. Filipp, J. Klepp, and H. Rauch, Phys. Rev. A **76**, 052108 (2007).
[16] H. Bartosik, J. Klepp, C. Schmitzer, S. Sponar, A. Cabello, H. Rauch, and Y. Hasegawa, Phys. Rev. Lett. **103**, 040403 (2009).
[17] D. A. Pushin, M. G. Huber, M. Arif, and D. G. Cory, Phys. Rev. Lett. **107**, 150401 (2011).
[18] F. Galve, G. L. Giorgi, and R. Zambrini, Europhys. Lett. **96**, 40005 (2011).
[19] W. K. Wootters, Phys. Rev. Lett. **80**, 2245 (1998).
[20] D. Zhou, G.-W. Chern, J. Fei, and R. Joynt, Int. J. Mod. Phys. B **26**, 1250054 (2012).
[21] T. Yu and J. H. Eberly, Science **323**, 598 (2009).

[22] T. Werlang, S. Souza, F. F. Fanchini, and C. J. Villas Boas, Phys. Rev. A **80**, 024103 (2009).
[23] A. Ferraro, L. Aolita, D. Cavalcanti, F. M. Cucchietti, and A. Acín, Phys. Rev. A **81**, 052318 (2010).
[24] F. F. Fanchini, L. K. Castelano, and A. O. Caldeira, New J. Phys. **12**, 073009 (2010).
[25] Y.-J. Zhang, X.-B. Zou, Y.-J. Xia, and G.-C. Guo, J. Phys. B **44**, 035503 (2011).
[26] V. F. Sears, *Neutron Optics* (Oxford University Press, New York, 1989).
[27] M. O. Scully, and K. Drühl, Phys. Rev. A **25**, 2208 (1982).
[28] Y. Aharonov, S. Popescu, D. Rohrlich, P. Skrzypczyk, New J. Phys. **15**, 113015 (2013).
[29] T. Denkmayr, H. Geppert, S. Sponar, H. Lemmel, A. Matzkin, J. Tollaksen, and Y. Hasegawa, Nat. Commun. **5**, 4492 (2014).
[30] Neutron Interferometry and Optics Facility; http://physics.nist.gov/majresfac/interfer/text.html.
[31] D. A. Pushin, M. Arif, M. Huber, and D. G. Cory, Phys. Rev. Lett. **100**, 250404 (2008).
[32] M. O. Abutaleb, D. A. Pushin, M. G. Huber, C. F. Majkrzak, M. Arif, and D. G. Cory, Appl. Phys. Lett. **101**, 182404 (2012).
[33] On loan from R. Pynn.
[34] R. Pynn, Physica B: Condens. Matter **356**, 178 (2005).
[35] D. A. Pushin, D. G. Cory, M. Arif, D. L. Jacobson, and M. G. Huber, Appl. Phys. Lett. **90**, 224104 (2007).